Flow Birefringence of Flexible Polymer Chains in Steady Shear Flow: A Brownian Dynamics Simulation

K. D. Knudsen* and A. Elgsaeter

Department of Physics, University of Trondheim—NTH, 7034 Trondheim, Norway

J. J. López Cascales and J. García de la Torre

Departamento de Química Física, Facultad de Química, Universidad de Murcia, 30071 Murcia, Spain

Received October 26, 1992; Revised Manuscript Received March 25, 1993

ABSTRACT: The steady-shear flow birefringence of flexible polymers modeled as Gaussian chains has been studied using Brownian dynamics simulation. The influence of flow rate and chain length on the two important parameters in flow birefringence measurements, the extinction angle χ and the birefringence Δn, has been investigated, and the power laws obtained have been compared with theoretical predictions. Hydrodynamic interaction (HI) has been included by means of the Rotne–Prager–Yamakawa tensor, and the simulation results have been compared with the no-HI case. For low shear rates inclusion of HI reduces the influence of flow on Δn and tan 2χ, while for high flow rates the chain behaves as in the no-HI case due to the large separation between beads and thereby elimination of flow interaction. For the shear compliance J, we obtain the value 0.29, which is higher than the theoretical value with preaveraged HI (0.20) and lower than that of the free-draining case (0.40), suggesting that preaveraged HI puts a too high weight on the HI contribution. The stress optical coefficient C has also been studied and found to be independent of chain length, shear rate, and HI.

Introduction

Flow birefringence has been known for many years as a sensitive tool for studying optical, conformational, and hydrodynamic properties of polymer solutions.[1] When polymer molecules are deformed and oriented in a shear flow, birefringence may result due to the induced optical anisotropy. The birefringence will in general consist of two parts, intrinsic birefringence and form birefringence.[2] The latter is always positive and will exist only if the index of refraction in the space occupied by the chain is different from that of the surrounding solvent, thus leading to optical anisotropy of the system if the chains are deformed and oriented. The intrinsic part, on the other hand, results from differential polarizability within a chain segment and exists even if there is no difference in the refractive index. It can be positive or negative depending on the chemical structure of the polymer. We will be treating the intrinsic birefringence, assuming that the form part is zero. Thus, in the following, birefringence refers to the intrinsic part.

There are, to our knowledge, few experimental results regarding the steady shear intrinsic birefringence of flexible chains. This may be due in part to complications with the simultaneous existence of form and intrinsic parts, which contribute in different manners to the overall birefringence[3] and therefore can be difficult to separate. There exist, however, theoretical predictions for the intrinsic birefringence of Gaussian chains, and in this study we will make use of the technique of Brownian dynamics to simulate the behavior of the steady state birefringence of a polymer chain of this type. We want to see if we are able to reproduce theoretical predictions regarding dependence on flow rate and chain length (molecular weight) and also to study the influence of hydrodynamic interaction between the beads in the chain.

Theory and Methods

Polymer Model. The polymer is modeled as a chain consisting of N spherical beads of radius σ joined by $N-1$ massless connectors. The orientations of the connectors are independent. The friction force on a bead due to the surrounding solvent is $\mathbf{F} = \zeta\mathbf{v} = 6\pi\eta_s\sigma\mathbf{v}$, where $\mathbf{v}$ is the velocity of the bead relative to the solvent, and η_s is the solvent viscosity. In the Rouse model, which we will be using, the connector is a Hookean spring with a stretching force $\mathbf{F}_j^E = -H\mathbf{Q}_j$, H being the force constant and $\mathbf{Q}_j$ being the vector between beads j and $j+1$.

If the root mean square connector length is b, the mean square end-to-end distance $\langle r^2\rangle_0$ for this chain in equilibrium (and not considering excluded volume effects; i.e., we are assuming θ-solvent) is $\langle r^2\rangle_0 = (N-1)b^2$. We will make use of the mean square radius of gyration $\langle S^2\rangle$ to monitor the overall extension of the chain and employ it in a relative form

$$\delta = \langle S^2\rangle/\langle S^2\rangle_0 - 1 \tag{1}$$

where the subscript 0 refers to the equilibrium value. It can be shown[4] that $\langle S^2\rangle_0 = (N^2-1)b^2/6N$, so that $\langle S^2\rangle_0$ is close to $\langle r^2\rangle_0/6$ for large N.

The optical behavior of our model is that of the Kuhn–Grün theory extended for flow birefringence by Zimm.[5] The polarizability along and perpendicular to a bond vector (Gaussian spring), γ_1' and γ_2', respectively, then depends on the spring elongation as

$$\gamma_1' = p + 2qb^2$$

$$\gamma_2' = p - qb^2 \tag{2}$$

where b is the spring length. The two parameters p and q are constants independent of spring elongation. The parameter p is given by $p = (\alpha_1 + 2\alpha_2)/3$, where α_1 and α_2 are the polarizabilities along and perpendicular to the segments making up the Gaussian spring, depending on the chemical structure of the segment. Thus, p can be viewed as an average intrinsic polarizability. The other parameter is given by $q = (\alpha_1 - \alpha_2)/5b_0^2$, where b_0 is the equilibrium spring length. The differential polarizability of the spring is then $\gamma_1' - \gamma_2' = 3(\alpha_1 - \alpha_2)b^2/5b_0^2$, depending

* To whom correspondence should be addressed.

0024-9297/93/2226-3851$04.00/0

on the square of the spring length. When there is no deformation (shear rate approaches zero), this expression is equal to $3(\alpha_1 - \alpha_2)/5$, i.e., independent of spring length.

We will make use of the intrinsic viscosity of the chain molecule for some calculations. The viscosity in simple shear $v = v_x = gy$ is given by $\eta = \tau_{xy}/g$, where τ_{xy} is the stress and g is the shear rate. If we then use the expression for the strain tensor given by Bird et al.,[4] we obtain a formula for calculating the intrinsic viscosity at shear rate g

$$[\eta] = \sum_j \frac{N_A \langle Q_{jx} F_{jy}^E \rangle}{\eta_s g M} \tag{3}$$

where N_A is Avogadro's number and M is the molecular weight, the latter being proportional to mN, where m is the bead mass.

Flow Birefringence. We assume a polymer solution which is subjected to a simple shear flow, produced by relative displacement of the x,z planes. The flow velocity is simply $v_x = gy$, $v_y = v_z = 0$. The shear rate g is also conveniently expressed in a reduced form containing the intrinsic viscosity at zero shear

$$\beta = \frac{M\eta_s[\eta]_0}{RT} g \tag{4}$$

The light beam that monitors the birefringence is assumed to propagate along the z direction.

The excess birefringence of a polymer solution with respect to that of the pure solvent is given by

$$\Delta n = Q\nu\Delta\Gamma \tag{5}$$

where $\Delta\Gamma$ is the difference of the components along the principal axes of the conformational average of the polarizability tensor. ν is the number of polymer molecules per unit volume, given by $\nu = cN_A/M$, where c is the mass concentration of the polymer. Q is a quantity whose particular form depends on the system of units used and how the internal field is treated; in any case it will contain only numerical constants and the refractive index of the solution.

If the polarizabilities of the individual springs (eq 2) are summed, we get the polarizability of the whole molecule, and the conformational average of this is the polarizability tensor Γ. The differential polarizability along the principle axes, $\Delta\Gamma$, is then given by[6]

$$\Delta\Gamma = 3q[(\langle x^T A x\rangle - \langle y^T A y\rangle)^2 + 4\langle x^T A y\rangle^2]^{1/2} \tag{6}$$

where x,y are the positions of the beads in the chain and A is a transformation matrix.[6]

Another quantity that is experimentally measurable is the extinction angle, χ, which is equal to the smaller angle between the principal axes of the polarizability tensor Γ and the x axis (stream lines). Diagonalization of the polarizability tensor gives[6] an equation for $\tan 2\chi$

$$\tan 2\chi = \frac{2\langle x^T A y\rangle}{\langle x^T A x\rangle - \langle y^T A y\rangle} \tag{7}$$

With random distribution of polymer segments, the two parts in the denominator of eq 7 are equal; thus $\chi = 45°$. As the segments align in the direction of the flow, χ approaches 0°.

The expressions above (eqs 6 and 7) are adequate for calculating the extinction angle and birefringence (i.e., $\Delta\Gamma$) in a computer simulation. It may be convenient to express the latter quantity in a reduced form, $\Delta\Gamma' = \Delta\Gamma/3qb^2$, i.e., eq 6 without $3q$ and with coordinates in units of b.

Stress Optical Relation. For certain systems there may be a proportionality between the applied shear stress and the resulting birefringence due to coaxiality of the corresponding tensors. This is formulated in the stress optical law

$$\Delta n = C\Delta p \tag{8}$$

where Δp is the difference in stress along the principal axes of the stress tensor, and C is the stress optical coefficient.

A commonly used expression for C reads[3]

$$C = \frac{4\pi(n_s^2 + 2)^2}{45kTn_s}(\alpha_1 - \alpha_2) \tag{9}$$

where n_s is the refractive index of the solvent, T is the temperature, and k is the Boltzmann constant. Expressions for C in terms of the refractive index and the polarizability of polymer segments can be found in the literature.[3,7]

Equation 8 can be transferred to the laboratory system, giving two equations[3]

$$\Delta n \sin 2\chi = 2C\tau_{xy}$$

$$\Delta n \cos 2\chi = C(\tau_{yy} - \tau_{xx}) \tag{10}$$

where we have assumed that the solvent does not contribute to the birefringence.

The intrinsic birefringence is defined as

$$[n] = \lim_{c\to 0} \frac{\Delta n}{cg\eta_s} \tag{11}$$

where c is the concentration. If we make use of the above expression together with that for the intrinsic viscosity

$$[\eta] = \lim_{c\to 0} \frac{\eta - \eta_s}{c\eta_s} \tag{12}$$

eq 10 (the upper part) can be written

$$[n]/[\eta] = 2C/\sin 2\chi \tag{13}$$

where we have used $\tau_{xy} = g(\eta - \eta_s)$.

In the limit of $g = 0$, $\sin 2\chi$ will approach zero,[7] and we can write

$$[n]_0/[\eta]_0 = 2C \tag{14}$$

As $[n]$ is proportional to $\Delta\Gamma$, we may use eq 13 to obtain a relation for calculating the relative stress optical coefficient at finite shear rate

$$\frac{C_1}{C_2} = \frac{\Delta\Gamma_1}{\Delta\Gamma_2}\frac{\sin 2\chi_1}{\sin 2\chi_2}\frac{[\eta]_2}{[\eta]_1} \tag{15}$$

where 1 and 2 mean two different systems, for example, chains with and without HI or with different numbers of beads. We will be using this expression to see if there is any influence of HI or chain length on the stress optical coefficient.

Power Laws. Evaluation of the averages in (7) gives for steady shear flow[6]

$$\tan 2\chi = \frac{1}{J}\frac{RT}{g\eta_s M[\eta]_0} \tag{16}$$

where R is the molar gas constant. J is a numerical constant which has been identified with the reduced form of a viscoelastic property, the steady shear compliance.[7] Theory predicts that $J = 0.40$ in the free-draining limit,[5]

where hydrodynamic interaction is neglected. With preaveraged hydrodynamic interaction, the Zimm model[5] gives $J = 0.205$, and the Pyun–Fixman calculation (high molecular weights) yields a value close to this,[8] $J = 0.194$.

Using the reduced shear rate β (eq 4), we can write

$$\tan 2\chi = (J\beta)^{-1} \tag{17}$$

For a Gaussian chain we have[4] that $[\eta]_0 \propto M$ without HI, and $[\eta]_0 \propto M^{1/2}$ with HI; thus $\beta \propto M^2 g$ (no HI) and $\beta \propto M^{3/2} g$ (HI). We therefore obtain the following power laws for the extinction angle:

$$\tan 2\chi \propto \beta^{-1}$$

$$\tan 2\chi \propto g^{-1} \qquad (M \text{ constant}) \tag{18}$$

$$\tan 2\chi \propto M^{-2} \qquad \text{(no HI)}$$
$$\propto M^{-3/2} \qquad \text{(HI)}$$

Evaluation of the averages in eq 6 gives[6]

$$\Delta\Gamma = K(N-1)g[\eta]_0 \operatorname{cosec} 2\chi \tag{19}$$

where K is a constant containing, among others, intrinsic optical parameters. The reason for the presence of the factor $N - 1$, instead of the bead number N, is that $\Delta\Gamma$ depends on the number of polarizable segments, being equal to $N - 1$. For large N, we can replace $N - 1$ by N and then use the expression for β to get

$$\Delta\Gamma \propto \beta \operatorname{cosec} 2\chi \tag{20}$$

With $\tan 2\chi = (J\beta)^{-1}$, we have

$$\operatorname{cosec} 2\chi = (1 + J^2\beta^2)^{1/2} \tag{21}$$

We then obtain

$$\operatorname{cosec} 2\chi \propto J\beta, \qquad \text{when } \beta \to \infty$$

$$\operatorname{cosec} 2\chi \propto 1 + \frac{J^2\beta^2}{2} \to 1, \qquad \text{when } \beta \to 0 \tag{22}$$

Now using once more that $[\eta]_0 \propto M$ (no HI) and $[\eta]_0 \propto M^{1/2}$ (HI), we obtain the following power laws for $\Delta\Gamma$. For high shear

$$\Delta\Gamma \propto \beta^2$$

$$\Delta\Gamma \propto g^2 \qquad (M \text{ constant}) \tag{23}$$

$$\Delta\Gamma \propto M^4 \qquad \text{(no HI)}$$
$$\propto M^3 \qquad \text{(HI)}$$

and for low shear

$$\Delta\Gamma \propto \beta$$

$$\Delta\Gamma \propto g \qquad (M \text{ constant}) \tag{24}$$

$$\Delta\Gamma \propto M^2 \qquad \text{(no HI)}$$
$$\propto M^{3/2} \qquad \text{(HI)}$$

Brownian Dynamics Simulation Scheme. The basis for simulating the trajectories in configuration space is the algorithm of Ermak and McCammon.[9] After a Brownian step of duration Δt, the new position vector $\mathbf{r}_i$ of a bead is obtained from the initial position $\mathbf{r}_i^0$ as

$$\mathbf{r}_i = \mathbf{r}_i^0 + \frac{\Delta t}{kT}\sum_j D_{ij}^0 \cdot \mathbf{F}_j^0 + \mathbf{v}(\mathbf{r}_i^0)\Delta t + \rho_i^0 \tag{25}$$

where the superscript 0 refers to the instant when the time step begins. $\mathbf{F}_j^0$ is the spring force on bead j, with contribution from the two springs $j - 1$ and j (except for beads 1 and N). D_{ij}^0 ($i,j = 1, \ldots, N$) is the ij block of the diffusion tensor. The parameter $\mathbf{v}(\mathbf{r}_i^0)$ is the velocity of the solvent at position $\mathbf{r}_i^0$ at the beginning of the time step. ρ_i^0 is a random vector with mean value 0 and variance–covariance equal to $2\Delta t D_{ij}^0$. The displacement of a bead thus has three contributions, that due to the spring forces on the bead, weighted with the diffusion coefficient, the contribution due to the solvent flow, and a stochastic part due to the impulses from the random motions of the solvent molecules surrounding the bead. In the simulations the basic algorithm (eq 25) is used with a second-order modification,[10] which has been shown to give improved calculation efficiency.

When hydrodynamic interaction between the chain units is taken into consideration, the Rotne–Prager–Yamakawa interaction tensor[11] is used for D_{ij}^0. If this interaction is neglected, D_{ij}^0 is just kT/ζ, and the above equation takes the form

$$\mathbf{r}_i = \mathbf{r}_i^0 + \frac{\Delta t}{\zeta}\sum_j \mathbf{F}_j^0 + \mathbf{v}(\mathbf{r}_i^0)\Delta t + \rho_i^0 \tag{26}$$

Dimensionless quantities are used throughout the simulations. Lengths are divided by b, forces by kT/b, and time by $\zeta b^2/kT$ (where $\zeta = 6\pi\eta_s\sigma$). Other dimensionless quantities follow from these definitions. The dimensionless shear rate, denoted g^*, will in this scheme be given by $g^* = (6\pi\eta_s\sigma b^2/kT)g$.

The trajectory of the molecule is simulated starting from a randomly generated conformation. The time step (in dimensionless units) was $\Delta t^* = 0.02$. A trajectory consists of a large number of Brownian steps (5×10^5–10×10^5), where the first part (usually 1×10^5 steps) is rejected, since it represents a transition from no-flow to steady state values. The remaining steps are used to calculate averages of the parameters of interest. Additional information on the simulation procedure can be found in López Cascales et al.[12]

Results and Discussion

Before presenting the results for the flow birefringence parameters, we will examine the variation of the conformation parameter δ with flow rate, with and without inclusion of hydrodynamic interaction (HI). This is done in part to compare with results from the literature and also to better be able to explain the behavior of the birefringence parameters examined later on.

Figure 1 shows the radius of gyration in relative form, δ, vs dimensionless shear rate g^* for a 12-bead Gaussian chain. At low shear the curves for the no-HI and the HI cases have the same slope, but different vertical positions. The introduction of HI reduces the value of δ, thus showing that the effect of HI is to reduce the overall chain dimensions. For high values of the shear rate, the two data sets superimpose. This behavior can be explained by taking into consideration that for a certain extension of the chain, that is, for a certain value of the shear rate, the hydrodynamic interaction loses its influence because of large separation between the beads, and the chain behaves as in the no-HI case.

In Figure 2, δ for two different chain lengths, $N = 12$ and $N = 20$, has been plotted vs the reduced shear rate

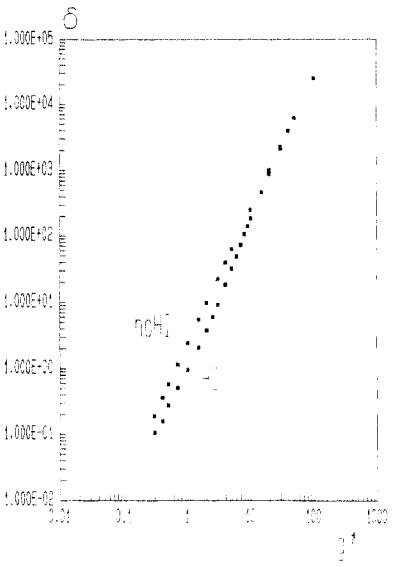

Figure 1. Relative radius of gyration, δ, vs shear rate (in dimensionless form), g^*, for a 12-bead Gaussian chain with and without hydrodynamic interaction (HI).

β. Figure 2A shows the no-HI case, and Figure 2B the HI case. The data sets for the different chain lengths superimpose because β includes the chain length dependent parameters M and $[\eta]$. Representing δ using β instead of the shear rate g along the abscissa thus makes it possible to obtain power laws independent of chain length. For the no-HI case, we obtain the relation $\delta = (0.15 \pm 0.01)\beta^{2.00\pm0.01}$. Thus, the exponent of β is 2. This accords perfectly with the theoretical result given by Pistoor and Binder[13] for Gaussian chains and large N, which can be written as $\delta = 0.15\beta^2$.

In the HI case (Figure 2B), we obtain for low β's the relation $\delta = (0.12 \pm 0.02)\beta^{1.95\pm0.07}$, and for high β's $\delta = (0.23 \pm 0.07)\beta^{2.1\pm0.1}$. Within the uncertainty of the simulation results, the exponents of β are thus still equal to 2. The value of the constant for low β's in the HI case (0.12) is in good agreement with the value 0.10 obtained in another work.[14] In the range $\beta \approx 10$–40 there occurs a transition where the hydrodynamic interaction loses its influence, as explained above while commenting on Figure 1. The relation between δ and β for high β's is therefore expected to be the same as in the no-HI case. Since the intrinsic viscosity at zero shear rate $[\eta]_0$ is different (lower) in the HI case than in the no-HI case, β will however be different in the two cases (eq 4), and as we have used the $[\eta]_{0,HI}$ value for β in Figure 2B, the constant in front of β for high β's (0.23) is higher than the corresponding value without HI. If we instead use the $[\eta]_{0,no\text{-}HI}$ value for this data set, the points will be displaced to higher β values, and we get a value of 0.15 for the constant, as in the no-HI case.

In summary, this study of the behavior of δ vs flow rate confirms the validity of our simulations and also demonstrates the influence of the hydrodynamic interaction.

The simulation results for the extinction angle vs β for chains with 12 and 20 beads without hydrodynamic interaction (not shown) adjust to the relation $\tan 2\chi = (2.4 \pm 0.3)\beta^{-0.99\pm0.02}$. That is, an exponent very close to −1 is obtained, in accordance with eq 18. The value of the constant in front of β also fits well with the theoretical prediction[5] of 0.4 given below eq 16 (1/2.4 = 0.42).

In the HI case, shown in a double-logarithmic plot in Figure 3, the data points can be seen to follow two straight lines, with a fairly broad transition zone around $\beta = 25$ where there is a vertical line displacement. This is the same transition between HI and no-HI behavior that has

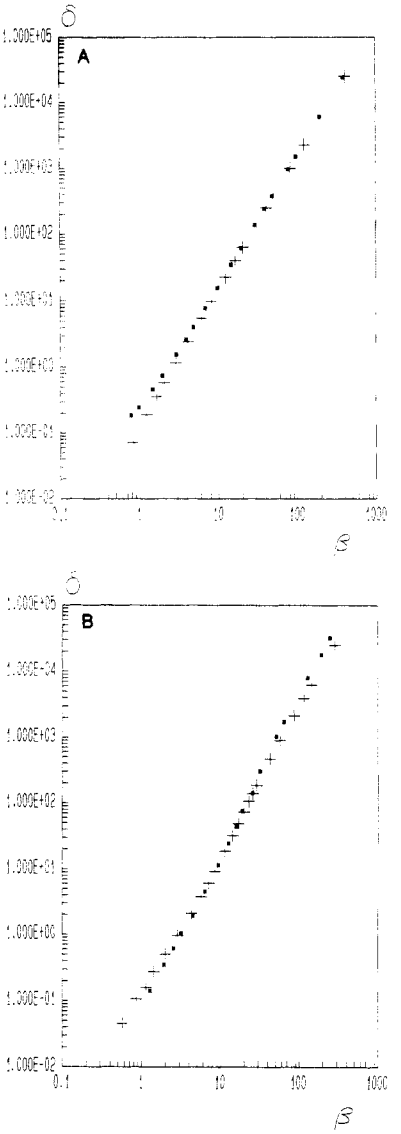

Figure 2. Relative radius of gyration, δ, vs reduced shear rate, β, for a 12-bead (+) and a 20-bead (■) Gaussian chain (A) without hydrodynamic interaction and (B) with hydrodynamic interaction.

been explained earlier for δ. For high β values, we obtained the relation $\tan 2\chi = (2.0 \pm 0.9)\beta^{-1.03\pm0.06}$, that is, an exponent close to that obtained for the no-HI case, as expected. When we adjust β using the $[\eta]_{0,no\text{-}HI}$ value, as done while discussing Figure 2B, we get a value of 2.9 for the constant in front of β, which deviates insignificantly (within the uncertainty of the simulations) from the value obtained in the no-HI case.

For low β values, the relation between the extinction angle and β is $(3.4 \pm 0.2)\beta^{-0.99\pm0.03}$. That is, a slope still close to −1 is obtained, in accordance with eq 18, but the value of the constant in front of β has increased in magnitude, showing that HI puts a higher value to the extinction angle and thus reduces the influence of flow on this parameter, as compared to the no-HI case. The value of the constant corresponds to $J = 0.29$ (1/3.4; see eq 17). As mentioned earlier, theoretical predictions[5] with preaveraged HI (Zimm model) give a value of 0.205 for this parameter, while in the free-draining limit, the value is 0.4. Our value of 0.29, obtained using a simulation without preaveraging (HI represented by the Rotne–Prager–Yamakawa tensor), seems to indicate that preaveraging puts a too high weight on the HI contribution.

Experimental results are fairly scarce for the parameter J, and the values obtained have usually been significantly

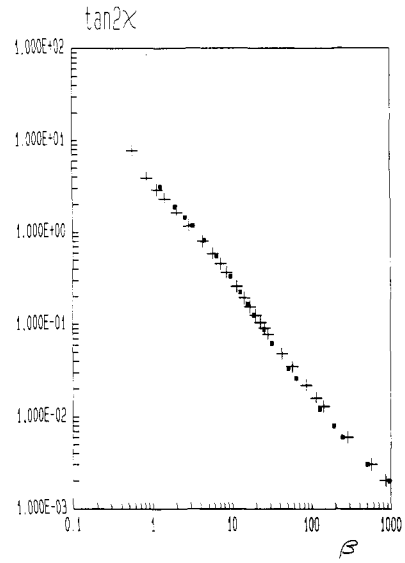

Figure 3. Extinction angle, tan 2χ, vs reduced shear rate, β, for a 12-bead (+) and a 20-bead (■) Gaussian chain with hydrodynamic interaction.

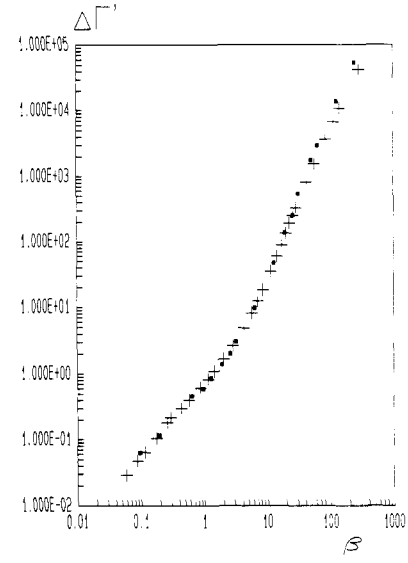

Figure 4. Differential polarizability in reduced form, $\Delta\Gamma'$, vs reduced shear rate, β, for a 12-bead (+) and a 20-bead (■) Gaussian chain with hydrodynamic interaction.

higher than the theoretical prediction, probably due to an insufficient sharpness of the investigated fractions.[7] The only experimental evidence that can be used to compare with our results is the careful measurement on polystyrene in Θ-solvent,[7] which gave values of J lying between the theoretical non-free-draining and free-draining limits (J = 0.2–0.4), and extrapolation to zero concentration gave the value J = 0.23. This is quite close to the theoretical prediction of 0.205 for non free draining according to the Zimm model but somewhat lower than the value obtained in our simulations (0.29) using nonpreaveraging.

For the differential polarizability $\Delta\Gamma'$, we ended up with two different regimes when obtaining the power laws—the low and high shear rate regimes (eqs 23 and 24). According to eq 22, a high shear rate means in this context $J\beta \gg 1$, which leads to $\beta \gg 5$ ($J \approx 0.2$). The simulation results for $\Delta\Gamma'$ for chains with 12 and 20 beads without HI (not shown) adjust for high β's to the relation $\Delta\Gamma' = (0.27 \pm 0.03)\beta^{2.00\pm0.01}$, and for low β's we get $\Delta\Gamma' = (0.77 \pm 0.01)\beta^{1.1\pm0.1}$. According to eqs 23 and 24, the exponents should be 2 and 1, respectively, and our results support this prediction. The coefficients in front of β will depend on the average value of the projection of the polymer segments onto the principal axis of the molecule (parentheses in eq 6), and we will not discuss these due to a lack of a theoretical value for this expression.

In the HI case, shown in Figure 4, we have in addition to the low and high shear regimes a transition zone between no-HI and HI behavior occurring in the same β region as for tan 2χ. For the highest β's we obtain the relation $\Delta\Gamma' = (0.47 \pm 0.04)\beta^{2.07\pm0.08}$, and low β's, $\Delta\Gamma' = (0.68 \pm 0.05)\beta^{0.98\pm0.12}$. Thus, also in the HI case the slopes are close to 2 and 1, respectively. This finding is as expected since the slopes for β are predicted to be independent of HI (eqs 23 and 24).

To study the influence of chain length, we have plotted in Figure 5 tan 2χ vs the number of beads N (log–log plot) for different shear rates, using chains with 5, 8, 12, and 20 beads. At high shear rates (lower curve, g^* = 40), the no-HI and HI curves overlap due to the loss of the HI effect as discussed earlier. We get here a slope of −1.88 ± 0.01, which is close to the theoretical no-HI value of −2 given in eq 18 (M and N are proportional quantities). To study the HI influence, we must use a lower value of the shear rate, and the upper curve in Figure 5 shows the

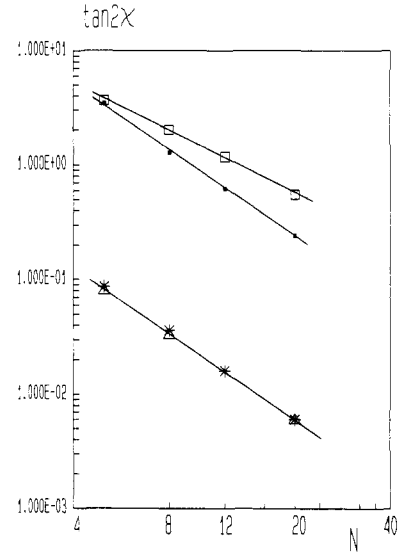

Figure 5. Extinction angle, tan 2χ, vs bead number N in the Gaussian chain with and without HI at high and low shear rate: (*) g^* = 40.0, HI; (△) g^* = 40.0, no HI; (■) g^* = 1.0, no HI; (□) g^* = 1.0, HI.

values obtained for g^* = 1.0. Here the slope of the line corresponding to the HI data is less than that of the no-HI data. In the no-HI case we still get a value close to −2 (−2.02 ± 0.07), but in the HI case the slope is now −1.30 ± 0.03, somewhat lower than the theoretical value of −1.5 given in eq 18.

In the same way as for tan 2χ, Figure 6 shows $\Delta\Gamma'$ vs number of beads N for high and low shear rates. Due to the factor $N - 1$ in the original expression for $\Delta\Gamma'$ (eq 19), power laws are best obtained for large values of N. The upper curve in Figure 6 shows data for g^* = 40, which satisfies the conditions for high shear given earlier, although poorer for the lower than for the higher N values ($\beta \propto N$). In this curve the data for the no-HI and the HI cases superimpose, just as for tan 2χ at high shear rate, and we get a slope of 3.9 ± 0.3, close to the theoretical value of 4 in eq 23. The lower curve in Figure 6 shows data for g^* = 0.1, which corresponds to the low shear region. Although the accuracy for this data set is somewhat lower than that for the high shear rate, we get different slopes for the HI and no-HI cases, with the HI curve less steep than the no-HI curve, in accordance with eq 24. The values

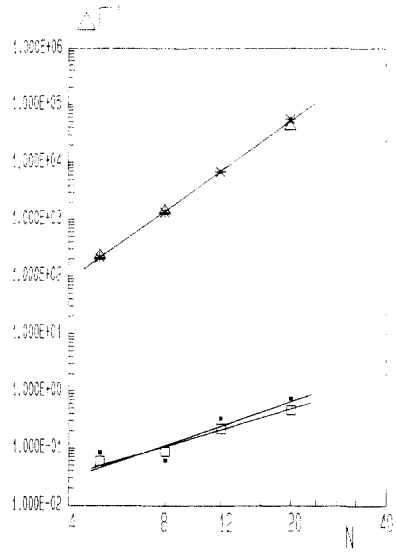

Figure 6. Differential polarizability in reduced form, $\Delta\Gamma'$, vs bead number N in the Gaussian chain with and without HI at high and low shear rate: (*) $g^* = 40.0$, HI; (△) $g^* = 40.0$, no HI; (■) $g^* = 0.1$, no HI; (□) $g^* = 0.1$, HI.

obtained for the slopes are 1.6 ± 0.2 and 1.9 ± 0.3, respectively.

Using eq 15, we have calculated the relation between the stress optical coefficient with and without hydrodynamic interaction, $C_{HI}/C_{no\text{-}HI}$, vs shear rate g^* for different chain lengths. This is shown in Figure 7A for chains with $N = 8$, 12, and 20 beads. The values obtained are all close to 1—the mean values are 1.00 ± 0.01, 1.02 ± 0.05, and 1.04 ± 0.04, respectively. Thus we observe no significant influence of HI on stress optical coefficient.

According to theory, the stress optical coefficient should depend only on the chemical structure of the chain ($\alpha_1 - \alpha_2$), solvent refractive index, and temperature (eq 9). It should be independent of hydrodynamic interaction, because the expression for the force used to calculate the stress tensor, and subsequently the stress optical coefficient, is assumed to contain all external forces as well as interactions with other parts of the chain.[7] This is however in contrast to some theoretical calculations, using nonpreaveraged HI but including another approximation in the hydrodynamic treatment (double-sum approximation[15,16]), which shows a reduction in the stress optical coefficient compared to the no-HI (free-draining) case. Calculations with preaveraged HI however give a stress optical coefficient that is independent of HI.[17]

Furthermore, the distribution function for the end points of the chain is eliminated when the stress optical coefficient is calculated;[7] thus it should also be independent of shear rate. As illustrated in Figure 7A, we observe no significant shear rate dependence over 3 decades of the shear rate. Finally, the stress optical coefficient should not depend on chain length; this is confirmed in our calculation of $C_{N=20}/C_{N=12}$ vs dimensionless shear rate g^*, shown in Figure 7B, where we get an average value of 1.01 ± 0.04 for this parameter.

The above results for the stress optical coefficient are in accordance with experimental data from flow birefringence measurements on flexible polymer chains. The relation Δn vs shear stress $\Delta\tau_{xy}$ is in general nonlinear.[1] However, when the product $\Delta n \sin 2\chi$ is plotted against the shear stress, a straight line results for a large range of shear rates,[7] indicating a simultaneous increase in Δn and decrease in χ, resulting in a shear rate independent stress optical coefficient. Regarding the possible dependence on chain length, experimental results for the stress optical

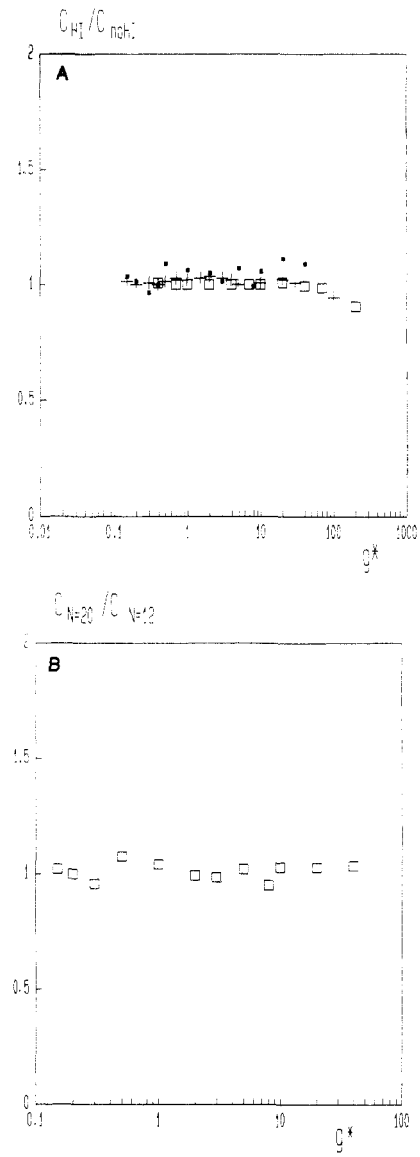

Figure 7. (A) Relative stress optical coefficient, $C_{HI}/C_{no\text{-}HI}$, vs shear rate, g^*, for Gaussian chains with different numbers of beads: (□) $N = 8$; (+) $N = 12$; (■) $N = 20$. (B) Relative stress optical coefficient, $C_{N=20}/C_{N=12}$, vs shear rate, g^*, for Gaussian chains with hydrodynamic interaction.

coefficient C vs molecular weight M have shown that C is independent of M for sufficiently high values of this parameter.[1]

Conclusion

Our simulation results for the power law behavior of the flow birefringence parameters tan 2χ and Δn (i.e., $\Delta\Gamma'$) are in good agreement with the theoretical predictions for Gaussian chains. The simulation results for the stress optical coefficient also agree with the theory regarding independency of chain length, shear rate, and hydrodynamic interaction.

Our value for the steady shear compliance J (0.29) is higher than that resulting from the Zimm (0.205) and the Pyun–Fixman (0.194) predictions and also somewhat higher than the only experimental result available for comparison (0.23). As experimental data on flow birefringence of flexible polymers are relatively scarce, it would be of value if this discrepancy could give stimulation to more experimental work in this field in the future.

It will be interesting to include effects like internal viscosity (kinetic chain stiffness), excluded volume, or

chain branching in the simulations of flow birefringence. Calculations have shown[7] that for example internal viscosity, in addition to causing a non-Newtonian behavior of the intrinsic viscosity, may reduce the influence of flow on the extinction angle and also change[3] the value of the steady shear compliance J. We felt however that before studying these effects it was important to investigate the simplest model of the Gaussian chain, as we have done in this work, and then later use this as a basis for studying influences of effects like those mentioned above.

Acknowledgment. This work has been supported by a travel grant from the Norwegian Research Council for Science and the Humanities (NAVF). K.D.K. acknowledges a postdoctoral fellowship from NAVF. We also acknowledge financial support from Grant PB90-0303 from Dirección General de Investigación Científica y Tècnica and Grant PB91-013 from Comunidad Autonoma, Región de Murcia, Spain.

References and Notes

(1) Tsvetkov, V. N.; Andreeva, L. N. *Adv. Polym. Sci.* **1981**, *39*, 35.
(2) Onuki, A.; Doi, M. *J. Chem. Phys.* **1986**, *85*, 1190.
(3) Munk, P. *Introduction to Macromolecular Science*; John Wiley & Sons: New York, 1989.
(4) Bird, R. B.; Curtiss, C. F.; Armstrong, R. C.; Hassager, O. *Dynamics of Polymeric Liquids*; John Wiley & Sons: New York, 1987; Vol. 2.
(5) Zimm, B. H. *J. Chem. Phys.* **1956**, *24*, 269.
(6) Yamakawa, H. *Modern Theory of Polymer Solutions*; Harper and Row: New York, 1971.
(7) Janeschitz-Kriegl, H. *Adv. Polym. Sci.* **1969**, *6*, 170.
(8) Pyun, C. W.; Fixman, M. *J. Chem. Phys.* **1965**, *42*, 3838.
(9) Ermak, D. L.; McCammon, J. A. *J. Chem. Phys.* **1978**, *69*, 1352.
(10) Iniesta, A.; Garcia de la Torre, J. *J. Chem. Phys.* **1990**, *92*, 2015.
(11) Yamakawa, H. *J. Chem. Phys.* **1970**, *53*, 436.
(12) López Cascales, J. J.; García de la Torre, J. *Polymer* **1991**, *32*, 3359.
(13) Pistoor, N.; Binder, K. *Colloid Polym. Sci.* **1988**, *266*, 132.
(14) López Cascales, J. J.; Navarro, S.; García de la Torre, J. *Macromolecules* **1992**, *25*, 3574.
(15) Freire, J. J.; García de la Torre, J. *Macromolecules* **1983**, *16*, 331.
(16) García de la Torre, J.; López Martínez, M. C.; Tirado, M. M.; Freire, J. J. *Macromolecules* **1984**, *17*, 2715.
(17) Fortelny, I. *Makromol. Chem.* **1982**, *183*, 193.